DFT-Parameterized Object Kinetic Monte Carlo Simulations of Radiation Damage

100

Enrique Martínez, María José Caturla, and Jaime Marian

Contents

1 Introduction 2458
2 Formulation and Mathematical Aspects of the Kinetic Monte Carlo Algorithm 2460
2.1 The Master Equation 2460
3 The Kinetic Monte Carlo Algorithm 2463
3.1 The Direct Method 2466
3.2 The First Reaction Method 2467
3.3 The Null Event Method 2467
4 Searching and Updating Algorithms 2468
4.1 Linear Search 2468
4.2 Binary Search 2469
4.3 Constant Time Search 2469
5 Object Kinetic Monte Carlo Methods 2470
6 Density Functional Theory to Calculate Propensities 2470
7 Examples 2473
7.1 Microstructural Evolution in α-Fe Under Irradiation 2473
7.2 Microstructural Evolution in W Under Fusion Conditions 2476

E. Martínez (✉)
Material Science and Technology Division, MST-8, Los Alamos National Laboratory, Los Alamos, NM, USA
e-mail: enriquem@lanl.gov

M. J. Caturla
Departamento de Física Aplicada, Facultad de Ciencias, Fase II, Universidad de Alicante, Alicante, Spain

J. Marian
Department of Materials Science and Engineering and Department of Mechanical and Aerospace Engineering, University of California, Los Angeles, CA, USA

Department of Mechanical and Aerospace Engineering, University of California, Los Angeles, CA, USA

© Springer Nature Switzerland AG 2020

W. Andreoni, S. Yip (eds.), *Handbook of Materials Modeling*,
https://doi.org/10.1007/978-3-319-44680-6_137

8 Limitations of the Method 2482
9 Conclusions 2483
References 2484

Abstract

Materials for nuclear applications are subjected to extremely stringent conditions. The incoming energetic particles create different types of defects in the material that modify the system microstructure. These defects diffuse and interact with each other and pre-existing features in the material, leading to alterations of the material properties, and even to failure. To deploy reliable materials for such extreme applications, a deep understanding of the microstructural changes and their relation to material properties is critically required. Synergistic experimental and theoretical studies are paramount to gain such crucial knowledge. In this work we review one theoretical venue developed over the years to first understand and then predict the material response upon irradiation: an object kinetic Monte Carlo (OKMC) approach parameterized to first-principles data. We review the theory behind the kinetic Monte Carlo (KMC) algorithm and the specifics of the OKMC as a mesoscale methodology. We describe density functional theory (DFT) as an ab initio approach that can accurately calculate parameters required by the OKMC as input data to be able to analyze the microstructure evolution of the system. Finally, we show two applications lengthily studied in the literature: the microstructural evolution of both ferritic steels and tungsten under diverse irradiation conditions.

1 Introduction

Irradiation has the potential to significantly alter the atomic structure of the material being irradiated. As energetic particles collide with the underlying atomic structure, extra energy is deposited in the material generating a sequence of structural modifications that are commonly denoted as defects. It is the evolution of these defects and their coupling with the material that dictate the resilience of the material to such irradiation conditions. Defects at the electronic level are known to vary the cohesive properties of the material (Correa et al. 2012; Draeger et al. 2017) and are usually characterized by short existence time on the order of femtoseconds. Defects at the atomic level, such as vacancies and interstitials, may also be created during the irradiation process. These structural defects are characterized by much longer lifetimes compared to electronic defects, during which these defects can migrate and interact with one another, generating new microstructural features that modify the material properties, and may eventually lead to failure. The time and length scales required to study the evolution of the irradiation-created defects exceed that attainable by molecular dynamics (MD) calculations. This is because MD solves Newton's equations of motion for an ensemble of atoms using an integration time step on the order of femtoseconds. This implies that the total number of steps

needed to reach simulated times of hours is around 3.6×10^{18}, far beyond the current computational capabilities. Accelerated MD (AMD) algorithms (Voter 1997, 1998; Sørensen and Voter 2000) extend the physical time that can be studied using MD approaches and provide good insights into complex mechanisms, but, because they also rely on a full description of the interatomic forces, their application is still limited in the system size as well as the simulated time. The kinetic Monte Carlo (KMC) algorithm (Elcock and McCombie 1958; Elcock 1959; Young and Elcock 1966; Bortz et al. 1975; Gillespie 1976, 1977; Voter 2007) also called the Stochastic Simulation Algorithm provides a methodology to overcome the MD time limitation. The scope of applications for KMC is extraordinarily wide, ranging from epidemiology and population kinetics to surface growth or radiation damage. This chapter reviews the time evolution of this last type of defects generated under irradiation as analyzed theoretically with a computational tool called object kinetic Monte Carlo (OKMC).

The specific type of defects generated under irradiation and the spatial correlations between them depend on the irradiation conditions and the material subjected to irradiation. Under electronic irradiation, usually Frenkel pairs, i.e., a vacancy and a self-interstitial, are formed (Was 2007). On the other hand, if irradiation is performed with neutrons, protons, or heavier ions with high enough energies, a thermal spike occurs in the material leading to a displacement cascade. Displacement cascades are commonly characterized by a low density core and a denser outer shell, i.e., the core is vacancy rich while the periphery is self-interstitial rich (Was 2007). The main goal of the OKMC is to study how these long-standing defects diffuse, react, and couple with pre-existing material's features to be able to first understand and then predict the microstructural changes taking place upon specific irradiation conditions. For such end, the OKMC needs the probabilities per unit time of all the possible events in the system. These probabilities are usually calculated in the context of transition state theory (TST) (Eyring et al. 1944; Voter and Doll 1984, 1985). According to TST, the rate for an event to happen follows an Arrhenius expression

$$\Gamma^{TST}_{\alpha\to\beta} = \nu^* \exp\left(-\frac{\Delta G_{\alpha\to\beta}}{k_B T}\right) \tag{1}$$

where ν^* is a pre-exponential factor, $\Delta G_{\alpha\to\beta}$ the activation free energy for the event that takes the system from state α to state β, k_B the Boltzmann constant, and T the temperature. This model relies on several assumptions: (i) the adiabatic approximation (Born-Oppenheimer) holds; (ii) the dynamics of the nuclei can be described with the classical equations of motion; (iii) the configuration at the initial minimum is at equilibrium, i.e., the system follows a Boltzmann distribution; and (iv) recrossing events at the transition state are negligible. The TST rate represents an upper bound to the true rate, $\Gamma^{TST}_{\alpha\to\beta} > \Gamma_{\alpha\to\beta}$, and can be adjusted considering dynamical corrections (Voter and Doll 1984, 1985). In the crystalline systems of most interest, at intermediate-to-low homologous temperatures, TST is commonly

approximated considering that the potential energy landscape is mostly harmonic (Vineyard 1957). In this approach, termed as harmonic TST (HTST), the rate is obtained through the expression

$$\Gamma_{\alpha\to\beta}^{HTST} = \frac{\prod_k^{3N} \omega_k^{\alpha}}{\prod_k^{3N-1} \omega_k^{ts}} \exp\left(-\frac{\Delta E_{\alpha\to\beta}}{k_B T}\right) \tag{2}$$

where ω_k^{α} are the normal mode frequencies in the initial minimum configuration (α), ω_k^{ts} are the normal mode frequencies when the system is at the transition state (ts), and $\Delta E_{\alpha\to\beta}$ is the activation potential energy for the particular event. Assuming that HTST holds, the big question is then how to obtain the activation energies and the vibrational frequencies to calculate the rate for the specific event. As we shall see in the following, for small defects and defect clusters containing less than around six individual defects, the most accurate tool that is commonly used is density functional theory (DFT) (Sholl and Steckel 2009), which considers electronic degrees of freedom and relies on fewer assumptions than classical empirical potentials. It is worth noting that free energies can also be computed within the DFT approach, which sometimes allows for the harmonicity constrain to be relaxed. Although more accurate, the computational cost constrains the calculations to fairly small samples and thus the size of the defects to be studied. The activation energy might depend on both the migration energy and a binding energy of the defect to a microstructural feature. For larger defects, the calculation of the rates usually relies on empirical potential approaches, such that interactions between defects are minimized and accurate parameters are obtained.

In this chapter we first review the theory behind the kinetic Monte Carlo algorithm to then particularize into the object-like KMC methods. Subsequently, we review the density functional theory approach and the calculations that can be done to obtain the mechanisms and the rates for such events to finally give some examples of OKMC simulations of microstructure evolution under irradiation.

2 Formulation and Mathematical Aspects of the Kinetic Monte Carlo Algorithm

The KMC algorithm gives one realization of the *Markovian master equation*. In this section we will review the definition and derivation of the master equation and its relation to the KMC method.

2.1 The Master Equation

2.1.1 Markov Processes

A Markov process (Kampen 1992) is a stochastic process with the property that the outcome of one step depends only on the outcome of the previous step. Formally, this can be written for n successive measurements as

$$P(x_n, t_n|x_1, t_1; \cdots; x_{n-1}, t_{n-1}) = P(x_n, t_n|x_{n-1}, t_{n-1}) \tag{3}$$

That is, the conditional probability density P to find the system in a state defined by x_n at time t_n, given by the value x_{n-1} at t_{n-1}, is uniquely determined and is not affected by any knowledge of the values at earlier times. P is called the transition probability, and x_n and t_n are two stochastic variables representing the measure and the time of the process.

A Markov process is fully determined by the two functions $P(x_1, t_1)$ and $P(x_2, t_2|x_1, t_1)$; the whole process can be constructed from them. For instance, taking $t_1 < t_2 < t_3$

$$\begin{aligned} P(x_1, t_1; x_2, t_2; x_3, t_3) &= P(x_1, t_1; x_2, t_2)P(x_3, t_3|x_1, t_1; x_2, t_2) \\ &= P(x_1, t_1)P(x_2, t_2|x_1, t_1)P(x_3, t_3|x_2, t_2) \end{aligned} \tag{4}$$

Continuing with this logic, one finds successively all P_n. This property makes Markov processes manageable, which is the reason why they are so useful in applications.

Integrating Eq. 4 over x_2 and dividing by $P(x_1, t_1)$, one obtains for $t_1 < t_2 < t_3$

$$P(x_3, t_3|x_1, t_1) = \int P(x_3, t_3|x_2, t_2)P(x_2, t_2|x_1, t_1)dx_2 \tag{5}$$

This is the Chapman-Kolmogorov equation. It is an identity which must be obeyed by the transition probability of any Markov process. The time ordering is essential: t_2 lies between t_1 and t_3. Two important remarks are as follows:

1. Two different Markov processes can describe the same physical system, depending on the level of coarseness of the description.
2. A Markov process is not restricted to one-component processes. For any r-component stochastic process, one may ignore a number of components, and the remaining s components again constitute a stochastic process. But, if the r-component process is Markovian, the process formed by the $s < r$ components in general is not. Vice versa, if a certain physically given process is not Markovian, it is sometimes possible by introducing additional components, to embed it in a Markov process. These additional components serve to describe explicitly information that otherwise would be contained implicitly in the past values of the variables.

As a matter of fact, in general, any closed isolated physical system can be described as a Markov process introducing all microscopic variables as components of the process. The key problem is to find a small set of variables which evolution can be described as a multicomponent Markov process. This reduction to a smaller number of variables is called “contraction” or “projection” (Kampen 1992).

2.1.2 Derivation of the Master Equation

Consider a Markov process in which the transition probabilities only depend on the time difference $\tau = t_2 - t_1$ such that $P(x_2, t_2|x_1, t_1) = T_\tau(x_2|x_1)$. The Chapman-Kolmogorov Eq. 5 for T_τ is a functional relation, which is not easy to handle in actual applications. The master equation is a more convenient version of the same equation: it is a differential equation obtained by going to the limit of vanishing time difference τ. It can be shown (Kampen 1992) that $T_\tau(x_2|x_1)$ for small τ has the form

$$T_\tau(x_2|x_1) = (1 - a_0\tau)\delta(x_2 - x_1) + \tau W(x_2|x_1) + \mathcal{O}(\tau) \tag{6}$$

Here $W(x_2|x_1)$ is the transition probability per unit time from x_1 to x_2, and hence

$$W(x_2|x_1) \geq 0 \tag{7}$$

The coefficient $(1 - a_0\tau)$ in front of the delta function is the probability that no transition takes place during τ; hence

$$a_0(x_1) = \int W(x_2|x_1)dx_2 \tag{8}$$

The Chapman-Kolmogorov Eq. 5 can be written as

$$T_{\tau+\tau'}(x_3|x_1) = [1 - a_0(x_3)\tau']T_\tau(x_3|x_1) + \tau' \int W(x_3|x_2)T_\tau(x_2|x_1)dx_2 \tag{9}$$

Dividing by τ', go to the limit $\tau' \to 0$, and use Eq. 8

$$\frac{\partial}{\partial\tau}T_\tau(x_3|x_1) = \int \{W(x_3|x_2)T_\tau(x_2|x_1) - W(x_2|x_3)T_\tau(x_3|x_1)\}dx_2 \tag{10}$$

which is a differential form of the Chapman-Kolmogorov equation, known as the master equation. For a discrete Markov chain with index n, this equation reduces to

$$\frac{\partial P(x,t)}{\partial t} = \int \{W(x|x')P(x',t) - W(x'|x)P(x,t)\}dx' \tag{11}$$

If the range of $X = (x_1; x_2; \cdots; x_n)$ is a discrete set of states, the equation reduces to

$$\frac{\partial p_n(t)}{\partial t} = \sum_n \{W_{nn'}p_{n'}(t) - W_{n'n}p_n(t)\} \tag{12}$$

which represents a rate equation (gain-loss equation) for the probabilities of the separate states n. The first term is the gain of state n due to transitions from other

states n', and the second term is the loss due to transitions from n into other states. Remember that $W_{nn'} \geq 0$ when $n \neq n'$ and that the term with $n = n'$ does not contribute to the sum (Kampen 1992).

Equation 12 can be written in a more compact form when the following matrix $\mathbb{W}$ is defined

$$\mathbb{W}_{nn'} = W_{nn'} - \delta_{nn'} \left(\sum_{n''} W_{n''n} \right) \tag{13}$$

Then Eq. 12 can be written

$$\dot{p}_n(t) = \sum_{n'} \mathbb{W}_{nn'} p_{n'}(t) \tag{14}$$

Formally the solution of Eq. 14 with given initial $p_n(0)$ may be written

$$p_n(t) = \exp\{t \cdot \mathbb{W}_{nn'}\} p_n(0) \tag{15}$$

$\mathbb{W}_{nn'}$ needs to follow

$$\mathbb{W}_{nn'} \geq 0 \quad \text{for n} \neq \text{ n'}; \tag{16}$$

$$\sum_{n} \mathbb{W}_{nn'} = 0 \quad \text{for each n'}. \tag{17}$$

Equation 16 shows the fact that the probability of staying in state n' is simply 1 minus the probability of escaping. For a complete reference on the properties of these matrices, see, e.g., Kampen (1992).

A fundamental property of the master equation is that as $t \to \infty$, all solutions tend to the stationary solution. This statement is strictly true only for a finite number of discrete states. For an infinite number of states, there are exceptions, such as the random walk.

3 The Kinetic Monte Carlo Algorithm

In any particular case, the master equation is fairly easy to write; however, solving it is quite another matter. The number of problems for which the master equation can be solved analytically is very limited. In addition, the master equation does not readily lend itself to numerical solutions due to the number and nature of its independent variables.

In 1976 Daniel T. Gillespie published his seminal paper *A General Method for Numerically Simulating Stochastic Time Evolution of Coupled Chemical Reactions* (Gillespie 1976). In this work, Gillespie developed the main theory behind what is nowadays known as the kinetic Monte Carlo algorithm. We will follow his

derivation here since it is concise and very clear. In Gillespie's words: "The method is a systematic, computer-oriented procedure in which rigorously derived Monte Carlo techniques are employed to *numerically simulate* the very Markov process that the Master Equation describes analytically." That is, the method circumvents the need to solve analytically or numerically the master equation and gives what is usually called "one realization of the master equation" since one dynamic trajectory in phase space is obtained from it. If many trajectories are simulated, the obtained probability distribution complies with the master equation, and thus, in essence, the algorithm is a method to numerically solve the master equation that we have described in previous sections.

Gillespie developed this method to study chemical reactions. In general, the method is applicable to every process that can be modeled with the master equation, and hence, the constraints imposed to its derivation apply to the problems that can be solved with this algorithm; mainly, the process has to be Markovian (remember that every deterministic process is Markovian) and first order in time.

We want to solve the dynamic evolution of a system characterized by a set of states in phase space α, β, γ, etc. As mentioned above, it is the researcher's task to define phase space so to comply with the necessary constraints and, therefore, to be able to solve the problem at hand using the kinetic Monte Carlo methodology. The fundamental hypothesis of the stochastic formulation, and the only assumption to be made by the computational method, is that the probability that a particular transition occurs in the next time interval δt is equal to $c_{\mu\nu}\delta t + o(\delta t)$, where $o(\delta t)$ denotes unspecified terms which satisfy $o(\delta t)/\delta t \to 0$ as $\delta t \to 0$. Therefore

$$\begin{aligned} c_{\mu\nu}\delta t \equiv &\text{average probability, to first order in } \delta t, \\ &\text{that a particular transition } (\mu \to \nu) \text{ occurs.} \end{aligned} \tag{18}$$

We want to solve the probability for the system to be in state μ at time t, $\forall t$, and $P(\mu; t)$, knowing the initial probability distribution and the transition probabilities per unit time $c_{\mu\nu}$. It is worth mentioning that the master equation can be derived from Eq. 18 by using the addition and multiplication laws of probability theory to write $P(\mu; t+dt)$ as the sum of the probabilities of the different ways for the system to arrive at state μ at time $t + dt$:

$$P(\mu, t + dt) = P(\mu, t)\left[1 - \sum_{\mu}^{M} c_{\mu\nu} dt\right] + \sum_{\nu}^{M} c_{\nu\mu} P(\nu; t) dt \tag{19}$$

and therefore

$$\frac{\partial P(\mu, t)}{\partial t} = \sum_{\nu}^{M} c_{\nu\mu} P(\nu; t) - \sum_{\mu}^{M} c_{\mu\nu} P(\mu, t) \tag{20}$$

which is the master equation, with M as the total number of states.

The principal theoretical construct upon which the procedure is based is not the grand probability function $P(\mu, t)$, nor any of its derived quantities, but rather an entity which is called the *reaction probability density function*, $P(\tau, \mu\nu)$, which is defined as

$$\begin{aligned} P(\tau, \mu\nu)d\tau \equiv & \text{probability at time t that the next transition} \\ & \text{in volume V will occur in the differential} \\ & \text{time interval } (t+\tau, t+\tau+d\tau) \\ & \text{and will be transition } \mu \to \nu. \end{aligned} \tag{21}$$

$P(\tau, \mu\nu)$ is a joint probability density function on the space of the continuous variable $\tau(0 \leq \tau < \infty)$ and the discrete variable $\mu\nu(\mu\nu = \alpha \to \beta, \alpha \to \gamma, \ldots, \beta \to \alpha, \ldots)$. This joint probability is the product of $P_0(\tau)$, the probability at time t that no transition will occur in the time interval $(t, t+\tau)$, times $c_{\mu\nu}d\tau$, and the subsequent probability that transition $\mu \to \nu$ will occur in the next differential time interval $(t+\tau, t+\tau+d\tau)$:

$$P(\tau, \mu\nu)d\tau = P_0(\tau) \cdot c_{\mu\nu}d\tau \tag{22}$$

Note that we need not worry about more than one reaction occurring in $(t+\tau, t+\tau+d\tau)$, since the probability for this to happen is $o(d\tau)$. $P_0(\tau)$ can be obtained if the interval $(t, t+\tau)$ is divided into K subintervals of equal length $\epsilon = \tau/K$. The probability if nothing happened in the first subinterval ϵ is

$$\prod_{\mu\nu}^{M} \left[1 - c_{\mu\nu}\epsilon + o(\epsilon)\right] = 1 - \sum_{\mu\nu}^{M} c_{\mu\nu}\epsilon + o(\epsilon) \tag{23}$$

For the whole interval, we can then write

$$P_0(\tau) = \left[1 - \sum_{\mu\nu}^{M} c_{\mu\nu}\epsilon + o(\epsilon)\right]^K = \left[1 - \sum_{\mu\nu}^{M} c_{\mu\nu}\tau/K + o(K^{-1})\right]^K \tag{24}$$

In the limit of infinitely large K

$$P_0(\tau) = \exp\left[-\sum_{\mu\nu}^{M} c_{\mu\nu}\tau\right] \tag{25}$$

Substituting in Eq. 22, we obtain

$$P(\tau, \mu\nu) = c_{\mu\nu} \exp\left[-\sum_{\mu\nu}^{M} c_{\mu\nu}\tau\right] \tag{26}$$

The main goal of the KMC algorithm is to generate random points in phase space according to such probability density function. Three main methods have been developed to do so: (i) the direct method, (ii) the first reaction method (also called the first passage method), and (iii) the null event method.

3.1 The Direct Method

This method is based on the fact that any two-variable probability density function can be written as the product of two one-variable probability density functions. As such we can write $P(\tau, \mu\nu)$ as

$$P(\tau, \mu\nu) = P_1(\tau) \cdot P_2(\mu\nu|\tau) \tag{27}$$

where $P_1(\tau)d\tau$ is the probability that the next reaction takes place within the interval $[t + \tau, t + \tau + d\tau]$, independent of which reaction it might be. $P_2(\mu\nu|\tau)$ is the conditional probability that next event is $\mu\nu$ given that it occurs at time $t + \tau$. $P_1(\tau)d\tau$ is obtained summing $P(\tau, \mu\nu)d\tau$ over all possible events $\mu\nu$:

$$P_1(\tau) = \sum_{\mu\nu}^{M} P(\tau, \mu\nu) \tag{28}$$

Substituting this expression into Eq. 27 and solving for $P_2(\mu\nu|\tau)$

$$P_2(\mu\nu|\tau) = \frac{P(\tau, \mu\nu)}{\sum_{\mu\nu}^{M} P(\tau, \mu\nu)} \tag{29}$$

Substituting now the expression for $P(\tau, \mu\nu)$ given in Eq. 26 and defining $R = \sum_{\mu\nu}^{M} c_{\mu\nu}$, we obtain

$$P_1(\tau) = R \exp(-R\tau) \qquad (0 \leq \tau < \infty), \tag{30}$$

$$P_2(\mu\nu|\tau) = \frac{c_{\mu\nu}}{R} \qquad (\mu\nu = 1, 2, \ldots, M), \tag{31}$$

and we can now generate a random τ according to $P_1(\tau)$ and a random $c_{\mu\nu}$ from $P_2(\mu\nu|\tau)$ with the resulting pair $(\tau, c_{\mu\nu})$ distributed according to $P(\tau, \mu\nu)$. τ can be obtained drawing a uniformly distributed random number (ξ_1) in the interval $[0, 1)$ from the expression

$$\tau = \frac{1}{R} \ln \frac{1}{\xi_1} \tag{32}$$

while $c_{\mu\nu}$ can be obtained drawing a second random number (ξ_1) again uniformly distributed in [0, 1) and taking the event that satisfies

$$\sum_{\mu\nu}^{m-1} c_{\mu\nu} < \xi_2 \leq \sum_{\mu\nu}^{m} c_{\mu\nu} \tag{33}$$

3.2 The First Reaction Method

This method is based on the fact that the probability that at time t the event $\mu\nu$ occurs in the interval $(t+\tau, t+\tau+d\tau)$ irrespectively of all other possible events is given by

$$P_{\mu\nu}(\tau)d\tau = \exp\left(-c_{\mu\nu}\tau\right) \cdot c_{\mu\nu}d\tau \tag{34}$$

Therefore, independent times for each event might be drawn from such probability distribution using the same expression as before:

$$\tau_{\mu\nu} = \frac{1}{c_{\mu\nu}} \ln \frac{1}{\xi_{\mu\nu}} \tag{35}$$

where $\xi_{\mu\nu}$ is a random number to be drawn uniformly for each possible event. The actual next event is the one with the shortest time. This scheme generates a pair $(\mu\nu, \tau)$ that complies with the $P(\tau, \mu\nu)$ probability density function. Because the amount of random number needed is much larger than in the previous method, this algorithm is usually less efficient. However, recent implementations take advantage of spatial decompositions to accelerate the wall time for the system to evolve in time (Opplestrup et al. 2006).

3.3 The Null Event Method

algorithm is based on the introduction of a new type of event, usually denoted as a null event, which if chosen keeps the microstructure in its original state. This extra event can be added to each individual event such that all events have the same total rate (Gilmer and Bennema 1972) or can be added to a cumulative rate of a set of events (Hanusse and Blanche 1981). It can be shown that this algorithm solves the same master equation as the previous two methods and therefore can be used to study the microstructural evolution, that is, the algorithm follows the right dynamics. The advantage of this method is that the searching wall time to find the event is reduced considerably, even to zero, i.e., the CPU time scales as $O(1)$. However, the simulated time step decreases, since it is sampled from the same probability distribution with the extra rates due to the null events, $\tau = \frac{1}{R_{\text{null}}} \ln \frac{1}{\xi_1}$, with R_{null} the aggregate of all rates. This implies that the best computational efficiency will occur

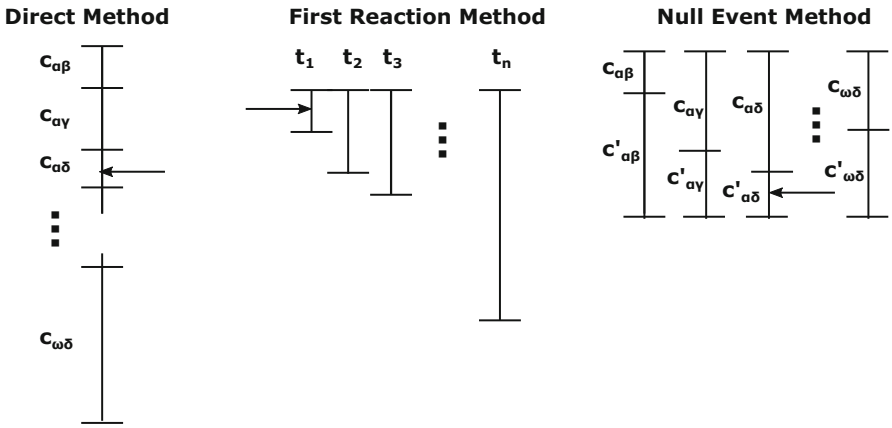

Fig. 1 Sampling approaches

for a minimum in the total null event rate (Chatterjee and Vlachos 2007). If the searching step in the direct method represents a large bottleneck in computational speed and the system is not significantly stiff (i.e., the total null event rate is not daunting), this algorithm can outperform the direct method.

Figure 1 shows schematics of the three sampling methods described above.

4 Searching and Updating Algorithms

Provided the rates are trivially calculated or are tabulated in advance, sampling Eq. 33 can represent the main computational bottleneck in KMC simulations. In general, the calculation of the rates is far from trivial, and several algorithms have been recently developed to calculate more accurately rates *on-the-fly* within a KMC scheme. This set of methods are usually denoted as adaptive KMC algorithms (Henkelman and Jonsson 2001; El-Mellouhi et al. 2008; Xu and Henkelman 2008). However, these methods are computationally demanding, and the total simulated time and the sample size remain limited. On the other hand, they are usually able (like MD or AMD) of obtaining the reaction mechanism without extra assumptions. In the context of irradiation to analyze the long-term microstructural evolution of the system under irradiation, the rates for the different events are usually pre-computed, and under these conditions, it is important to identify the possible different searching and updating algorithms that reduce the wall time in sampling Eq. 33 and updating the rates and its aggregate.

4.1 Linear Search

The linear search is the simplest algorithm to implement. It uses an array or list of possible events with an assigned rate that visits linearly, i.e., one by one in the list,

to calculate the cumulative rate, until Eq. 33 is satisfied. This method scales linearly with the number of events, i.e., $O(N)$ with N the total number of events. Grouping can be used to improve the efficiency in what has been denoted as n-level linear algorithms. In this case a set of events are grouped together and the cumulative rate computed in as many levels as wanted. Each search goes in general through a number of events that is $N_n \approx N^{1/n}$, with n the level of grouping. The wall time of this algorithms scales then as $nO(N_n)$, which can be considerably faster than the brute force linear search.

4.2 Binary Search

Binary searches rely on the generation of a tree data structure containing information about the rates (Gibson et al. 2000; Schulze 2002) to reduce the CPU time required to sample Eq. 33. In this structure, each node represents a cumulative propensity of the branches below it, such that the bottom nodes represent individual propensities for specific events. The number of levels in a tree will be at least $N_{level} = floor(\log_2(N))$. If this is the case, the tree is considered equilibrated, and the computational efficiency is maximum. The algorithm starts at the head node that contains the cumulative rate of the left branch. If the target rate is lower, the next search is performed in the children to the left of the head node, to the right otherwise. This process is repeated until the bottom of the tree is reached and the event identified. In this algorithm the CPU time scales as $O(\log_2(N))$; however, the pre-factor to keep the tree equilibrated might be significant, and, not in every situation, this algorithm is faster than the linear searches.

4.3 Constant Time Search

The main idea of this method is based on the null event (or rejection) algorithm, in which the need for searching is reduced to drawing an integer random number from a uniform distribution between $[1, N]$, with N the total number of possible events, which will directly point at the event to be performed, including a null event. A second random number must be generated to pick between the actual or the null events. The search does not depend on the number of events, N, and therefore scales as $O(1)$. In a stiff problem with significantly different rates, a grouping algorithm can be developed to minimize the amount of null events. This will resemble a combination between the n-level search with the extra addition of the null events. In this case the search would be $O(N_n)$, with N_n the number of groups. This null event (or padding) method could also be combined with a binary search to keep the tree balanced. A review of this method can be found in Slepoy et al. (2008).

Figure 2 shows a summary of the searching algorithms discussed above.

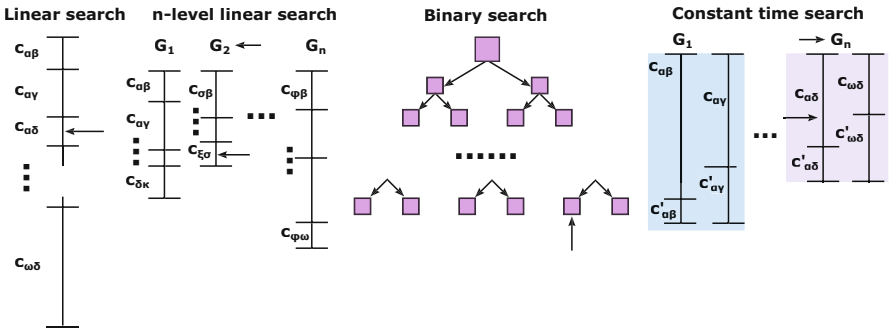

Fig. 2 Searching algorithms

5 Object Kinetic Monte Carlo Methods

The object kinetic Monte Carlo (OKMC) method uses a coarse-grained representation of the system to accelerate the wall time required to analyze its time evolution. In the context of materials under irradiation, the method averages out the underlying atomic structure to consider as possible event processes involving defects. Therefore, the algorithm follows the irradiation-created defects in time, solving for their migration and the interaction with one another and other kinds of features in the microstructure, such as grain boundaries, dislocations, alloying elements, or such. As it was mentioned in Sect. 1, TST is usually assumed to calculate the rates for each possible event, although, in general, experimental results or MD simulations can be also used to obtain such propensities, including dynamical corrections. The method results in a defect distribution evolving in time for a given initial microstructure (may be containing defect sinks such as interfaces or dislocations) under a given set of irradiation conditions, such as dose rate, temperature, pressure, and information about the nature of the defects created in the collision processes.

6 Density Functional Theory to Calculate Propensities

Density functional theory (DFT) is a mean field approach to solve the many-body Schrodinger equation (Hohenberg and Kohn 1964). It is based on the fact that the ground-state properties of a many-electron system are uniquely determined by an electron density that depends on only three spatial coordinates. As such, the many-body problem of M electrons with $3M$ spatial degrees of freedom is reduced to three spatial coordinates through the use of functionals of the electron density. DFT assumes that the electron dynamics are much faster than the nuclei and solves the ground-state electronic structure for a fixed positions of the nuclei, i.e., the

Born-Oppenheimer approximation is assumed to hold. Hohenberg and Kohn (1964) developed an energy functional for the system and demonstrated that the true ground state of such energy functional minimizes the functional. Subsequently, Kohn and Sham (1965) were able to reduce the many-body problem of interacting electrons in a static external potential to a solvable problem of noninteracting electrons evolving in an effective potential. The correctness of these methods mainly relies on the accuracy of this effective potential. This effective potential includes the external potential and the Coulomb interactions between electrons, with contributions from the exchange and correlation interactions. The simplest approach is the local-density approximation (LDA) that relies on the exact exchange energy for a uniform electron gas as given by the Thomas-Fermi model (Ceperley et al. 1980). More complex functionals for exchange and correlation have been developed and still are a very active field of research. One widely used example is the generalized gradient approximation (GGA) that incorporates information about the gradient of the electron density in the functionals to account for the non-homogeneity of the real electron density (Langreth and Mehl 1983; Becke 1988; Perdew et al. 1992). Hybrid functionals incorporating a portion of the exact exchange energy calculated from Hartree-Fock theory with the rest of exchange correlation from other sources are also extensively used. The problem of finding the ground-state electron density is variational and has to be solved iteratively in a self-consistent manner such that the effective potential and the wave functions are also obtained for such electron density.

DFT is widely used in chemistry and materials science to understand and predict the properties of complex systems under specific conditions. Although computationally more efficient than all-electron approaches, the solution of the DFT equations presents a computational bottleneck, which translates into limited system sizes and simulated times. In general, the computational scaling of this method is $O(n^3)$ with n the number of electrons since usually the diagonalization of the system Hamiltonian scales as n^3. The development of $O(n)$ methods is also a remarkably active research area (Niklasson et al. 2006; Witt et al. 2018).

In the context of materials under irradiation, this approach has been broadly used to estimate the properties of defects. Although usually calculated at 0 K, there have been some studies using ab initio MD to compute the required properties (Grabowski et al. 2007; Körmann et al. 2008; Grabowski et al. 2011; Glensk et al. 2015) at higher temperature. One of such properties is the defect formation energy. This is usually calculated as

$$E_{\text{for}}(D) = E\left[N_{\text{at}} + D\right] - (N_{\text{at}} + D)\mu \tag{36}$$

where D represents the defect, N_{at} is the number of atoms in the bulk system, and μ is the cohesive energy of the material. This formation energy might be used to estimate the equilibrium defect populations.

Another important quantity is the migration energy ($E_m(D)$), which is defined as the difference of the energy of the system at the saddle point and the initial state

for a defect hopping. To compute this migration energy, the system is forced to converge to the minimum energy path (MEP) between the initial and final states. If the initial and final states are known, methods like the drag method (Trushin 2005) or the nudged elastic band (NEB) (Henkelman and Jonsson 2000; Henkelman et al. 2000) are commonly used. If the final state is unknown a priori, the dimer method (Henkelman and Jonsson 1999) or the Lanczos method (El-Mellouhi et al. 2008) are usually preferred. Recently, advanced methods have been developed to improve the predictions obtained with the traditional methods, such as free-end NEB (Zhu et al. 2007) or free-end adaptive NEB (Zhang et al. 2016). This $E_m(D)$ will be used in the HTST expression (Eq. 2) to compute the migration rate. The pre-factor is usually assumed constant and close to the Debye frequency of the material. However, under certain conditions, it has been shown that the explicit calculation of the pre-factor might significantly change the event rate. One of such conditions arises when the system is under nonuniform strain, in which case the pre-factor can change by orders of magnitude (Uberuaga et al. 2007). Vineyard pre-exponential factors can also be calculated within DFT, although the computational expense is high.

Binding energies are also crucial for the method to be predictive. The binding energy characterizes the interaction between two or more species in the system. It is defined as the energy gain in a given reactions that can be exothermic or endothermic:

$$E^b_{X-Y}(A) = E[S + X + Y] + E[S] - (E[S + X] + E[S + Y]) \tag{37}$$

where $E^b_{X-Y}(A)$ denotes the binding energy of species X and Y in system S, $E[S+X+Y]$ is the energy of the system with the interacting species, $E[S]$ is the reference system, and $E[S + X]$ and $E[S + Y]$ are the reference systems with specie X and Y, respectively. Important binding energies are, for example, from single defects to clusters, between defects and impurities or alloying elements, and between defects and sinks (such as grain boundaries or dislocations). This binding energy enters in the activation energy for a dissociation process, altering the propensity for such reaction to occur. Expressions derived from elasticity theory are commonly used to fit the values obtained from DFT and extrapolate for larger cluster sizes (Perini et al. 1984).

The interaction radius is also an important parameter needed in the OKMC method. In general, it depends on the species and its size. Usually, empirical relations based on DFT data are used. For defect clusters, a common expression is $r_n = Z \cdot \left(\frac{3n\Omega}{4\pi}\right)^{1/3} + r_0$, where Z is a bias factor depending on the nature of the defect, n is the number of single defects in the cluster, Ω is the atomic volume, and r_0 is a constant usually obtained with DFT.

DFT has also been used to obtain threshold displacement energies in materials of interest, i.e., the minimum energy that needs to be given to an atom such that a stable Frenkel pair is formed. This approach has been employed to study the energetic threshold depending on the orientation in materials such as α-Fe (Olsson et al. 2016) and W (De Backer et al. 2016).

7 Examples

In this section we will show a couple of examples in which this method has been applied to analyze the evolution of the microstructure under irradiation. The first one is for ferritic/martensitic steels, which is of great importance in nuclear applications. The second example studies the defect evolution in tungsten (W) and the interaction of the irradiation-created defects with He created from (n, α) nuclear reactions and the incoming flux from the plasma ashes.

7.1 Microstructural Evolution in α-Fe Under Irradiation

Irradiation of a metal and subsequent annealing while measuring electrical resistivity can provide important information about basic processes related to defect migration and defect stability, data that can be calculated with DFT or other atomic-scale models as mentioned in the previous section. C. C. Fu et al. (2005) using event kinetic Monte Carlo with parameters from DFT simulated the resistivity recovery curve of Fe after electron irradiation and correlated these results to the different peaks observed in experiments performed by Takaki et al. (1983). Figure 3 shows the derivative of the number of defects (N) as a function of temperature obtained in this case with OKMC and the same parameters as in Fu et al. (2005) for a dose of $2 \times 10^{-6} dpa$ (dpa = displacements per atom). The locations of the peaks found experimentally in Takaki et al. (1983) are marked in the same figure with arrows. These simulations show that the first peak (named stage ID2) appears because of the recombination of correlated Frenkel pairs. In this case the vacancy and self-interstitial belong to the same Frenkel pair in such a way that with one single self-interstitial jump, these defects recombine. Recombination of defects gives rise to a decrease in the resistivity of the material and therefore a peak in the derivative of the curve. The second stage, named IE, also corresponds to the recombination between vacancies and self-interstitials but for pairs of defects that are far away from each other, so more than one jump of the self-interstitial must occur for the defects to recombine. This peak appears at a temperature that corresponds to that of self-interstitial migration. The next stage, stage II, is due to the migration of self-interstitial clusters, while stage III is due to vacancy migration.

In the case of an alloy, if the concentration is low, the alloying element can be treated explicitly in the OKMC approach by treating every alloy atom as a defect. As mentioned above, in the OKMC approach, there is no underlying lattice, so, in principle, these atoms will be distributed randomly within the simulation cell. All the possible events that these atoms can perform, interaction with vacancies or self-interstitials, formation of clusters, or migration must be specified with their appropriate rates. For the case of FeCr alloys, there is information obtained from DFT on small clusters (Olsson et al. 2007; Olsson 2009). One important defect formed in FeCr alloys is the mixed interstitial dumbbell, which has a lower migration energy than the self-interstitial cluster, but also a low binding energy

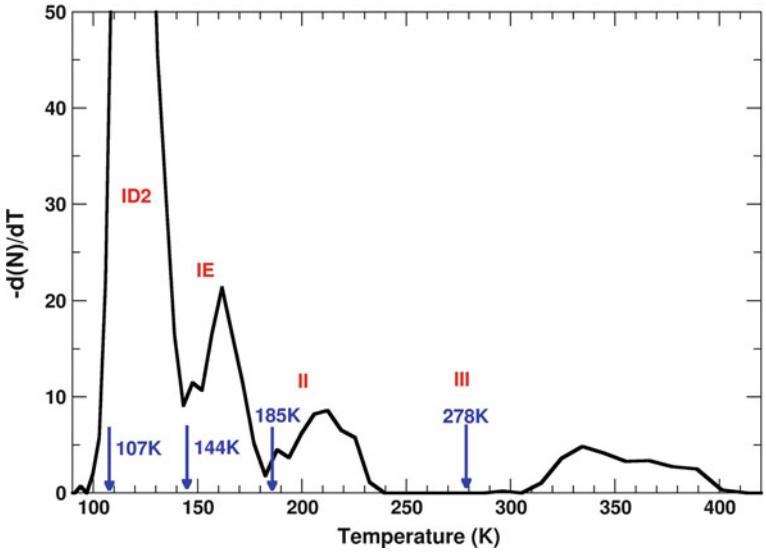

Fig. 3 Derivative of the number of defects as a function of temperature for electron irradiation of Fe at a dose of $2 \times 10^{-6} dpa$ from OKMC calculations and parameters from Fu et al. (2005)

(Domain et al. 2004). Experimentally, it is observed that in low-concentration alloys (between 0.01 and 0.1% Cr), the IE peak in the resistivity recovery measurements shifts toward lower temperatures and the shift increases with Cr concentration (Abe and Kuramoto 1999; Maury et al. 1987). Using an OKMC model with parameters from DFT as described in Gámez et al. (2011) that include the formation of mixed dumbbells (ICr) as well as other Cr clusters (I2Cr, ICr2, and I2Cr2), the shift was reproduced as it can be seen in Fig. 4. This figure shows the results for pure Fe and for FeCr at the three concentrations measured experimentally in Abe and Kuramoto (1999), 0.019 at%, 0.047 at%, and 0.095 at%), and how the IE peak moves toward lower temperatures with increasing Cr concentration in agreement with the experiments. The reason behind this shift is in fact the formation of the ICr mixed dumbbell.

One of the advantages of the OKMC approach is that system sizes larger than those in lattice KMC (LKMC) models can be simulated, typically cubes of hundreds of nanometers on each direction. This allows for calculations of damage accumulation as a function of irradiation to doses that can be achieved experimentally and to model the formation of clusters large enough to be visible under transmission electron microscopy (TEM). An example of these types of simulations that have been performed by several groups for different conditions, starting with the work of Heinisch (1990) (see, e.g., Domain et al. 2004; Malerba et al. 2008; Becquart and Domain 2010), is presented here. In this case, the accumulation of damage during continuous irradiation of Fe and Cu is simulated. Details of these calculations are

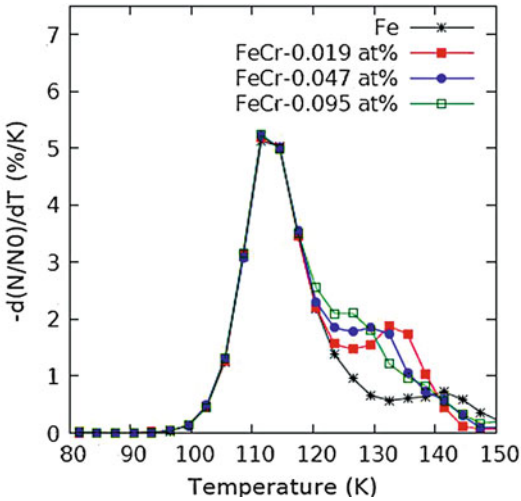

Fig. 4 Derivative of the number of defects as a function of temperature for electron irradiation of pure Fe and FeCr alloys of three different concentrations following the experimental work of Abe and Kuramoto (1999) obtained from OKMC and parameters from DFT (see Gámez et al. (2011) for details)

in Caturla et al. (2000). In brief, a database of collision cascades in Cu and Fe for 30 keV recoils obtained from molecular dynamics simulations is used as initial damage distribution. This picosecond time damage is very different in Fe and in Cu. Cu presents mostly clustered vacancies with surrounding self-interstitial clusters, while in Fe most of the vacancies are isolated or forming very small clusters. The values of migration energies and binding energies of defects used in the calculations were obtained from empirical potentials. Figure 5 shows the total concentration of visible clusters as a function of dose for the case of the two materials studied, Cu and Fe. Here, the visibility conditions were considered as follows: 20 defects for vacancies in Cu, equivalent to a stacking fault tetrahedra of 1.5 nm, 350 vacancies for a 1 nm void in Fe, and 50 self-interstitials for a 1 nm loop in Fe. This figure shows that there is an important difference in the damage accumulated in Fe vs. Cu, phenomenon also observed experimentally (Dai et al. 1997). The reason for this difference is related both to the initial damage distribution and the effect of impurities in these two materials. In Cu, where no impurities are considered in the simulation, most self-interstitials and self-interstitial clusters disappear through recombination with vacancies or at grain boundaries, and most of the damage is vacancy clusters, with an average size of about 28 vacancies which corresponds with a 2 nm stacking fault, in agreement with experimental observations (Zinkle and Farrell 1989). In Fe, self-interstitials are trapped by impurities, which result in visible clusters, while vacancies are too small to be observed under TEM (with less than 15 defects). In Fe most of the evolution of the clusters and growth to sizes that can be observed experimentally is going to occur through defect diffusion and defect coalescence. And the description of these interactions depends on the set of reactions that the user of the OKMC model has decided to consider as the important ones.

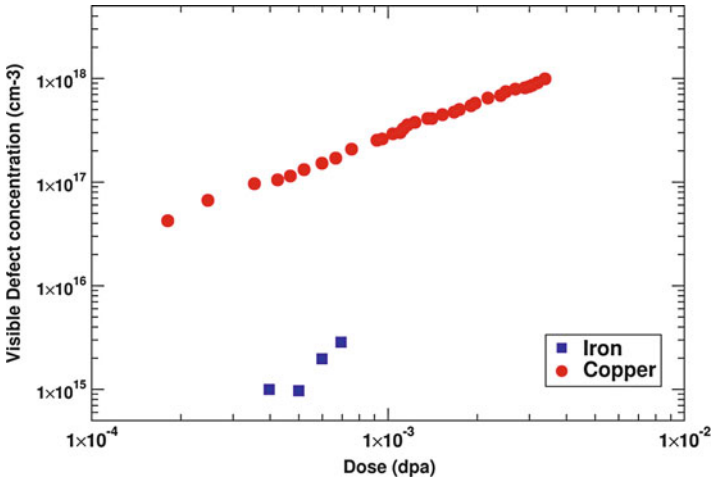

Fig. 5 Visible defect clusters as a function of irradiation dose for the case of Fe and Cu (see Caturla et al. 2000 for details)

7.2 Microstructural Evolution in W Under Fusion Conditions

Critical components in magnetic fusion reactors are required to have stringent properties including low neutron activation, high melting point, good thermomechanical properties, low sputter erosion, and low tritium retention/co-deposition. Tungsten (W) is the leading plasma-facing material (PFM) candidate due to its high melting temperature, low erosion rates, and small tritium retention. These advantages are unfortunately coupled with very low fracture toughness characterized by brittle transgranular and intergranular failure regimes, which severely restrict the useful operating temperature window and also create a range of fabrication difficulties. Exposure to He and H plasma leads to the formation of diverse microstructures (pits, holes, bubbles, nanostructured surface morphology termed as fuzz) (Baldwin and Doerner 2008) that severely limit its utilization. Therefore, understanding the mechanisms leading to the W failure is crucial to develop materials to be able to withstand the extreme environments posed by fusion energy generation.

DFT has been broadly used to obtain the data mentioned above and needed by the OKMC to evolve the microstructure. Using different DFT approaches, the formation energies of intrinsic defects have been calculated. The single vacancy (V) values in the literature range from ~3.1 to ~3.7 eV (Söderlind et al. 2000; Becquart and Domain 2007; Suzudo et al. 2014), while for self-interstitial atoms (SIA), the values depend on the configuration. Some discrepancy arises in the literature about the most stable configuration, with similar values for the ⟨111⟩ dumbbell, ⟨111⟩ crowdion, and a slightly rotated configuration, with values around ~9.6–9.7 eV (Nguyen-Manh and Dudarev 2006; Suzudo et al. 2014) and ~10.41 (Becquart and Domain 2007) depending on the approach. Binding energies of individual defects

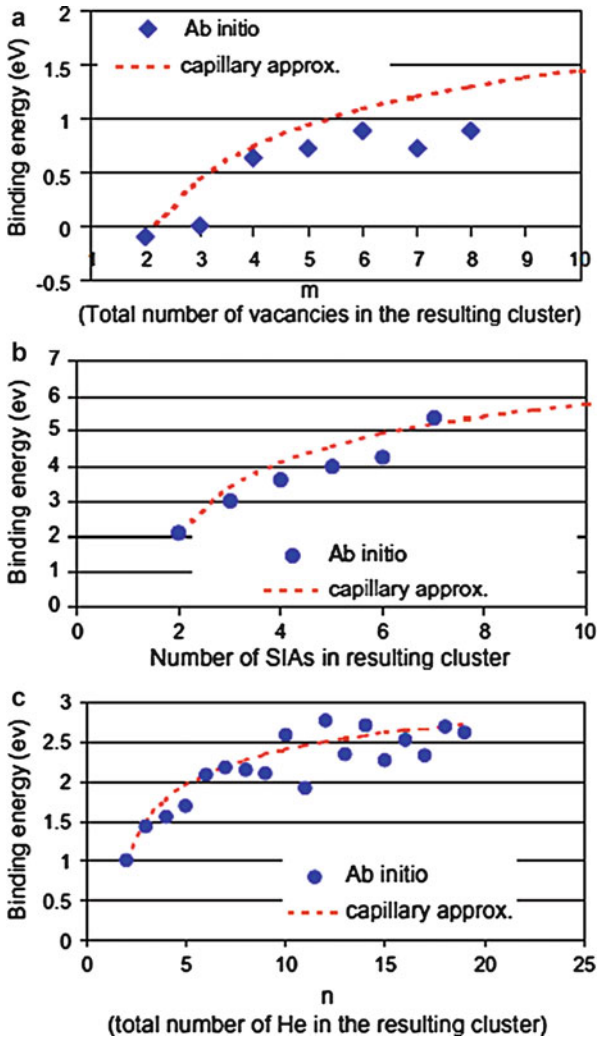

Fig. 6 Binding energies of individual defects to their clusters for (**a**) vacancies, (**b**) self-interstitial atoms, and (**c**) He atoms (Becquart and Domain 2010)

to defect clusters are also required. Becquart et al. calculated the ones for vacancies and interstitials using their DFT approach and use a capillary law for large defect clusters (>8 V for vacancy clusters and >7 SIA for interstitial clusters). Figure 6a and 6b shows the results for vacancies and self-interstitials, respectively. We observe that the capillary approximation fits well the ab initio data. One of the puzzling results in W is that the binding energy of two individual vacancies is repulsive, i.e., vacancies do not want to aggregate.

The migration energies for the intrinsic defects and their clusters are also needed. For individual defects, several sources are available in the literature (Becquart and Domain 2010; Suzudo et al. 2014; Huang et al. 2016), all describing single

vacancies with a large migration energy (∼1.7 eV), while SIAs show a remarkably small migration barrier (∼0.005–0.056) eV. Becquart et al. (2010) proposed an expression for the diffusion constant of defect clusters. In the case of vacancy clusters, the attempt frequency is given by $\nu = \nu_0(q^{-1})^{n-1}$, with $\nu_0 = 6 \times 10^{12}\ \mathrm{s}^{-1}$ constant and equal for V and SIA, $q = 1000$, and n the number of individual defects in the cluster. Based on this model, Castin et al. (2017) have recently proposed an extension to account for the effect of grain boundaries and carbon impurities. The authors presented a sensitivity analysis of the parameters that mostly influence the onset of void swelling using their in-house OKMC code called MATEO concluding that the presence of carbon impurities in the W matrix strongly influences the kinetics of void formation due to the strong binding interaction between carbon and vacancies. They also showed the importance of correlated recombination after cascade events in the microstructure evolution. Mason et al. (2014) used a different parametrization of formation and migration of clusters to study loop accumulation and their interactions in a W thin film. In this case, they explicitly added elastic interactions between defects to analyze the evolution of collision cascades and compare the effect of impurity trapping and elastic trapping concluding that elastic loop trapping within a cascade can stabilize large loops at high temperatures, while they shrink at low temperatures. On the other hand, small loops glide to the surface at high temperature, hence accounting for the experimentally observed reduction in total loop density and the change in the loop size distribution (Fig. 7).

As mentioned above, the study of the effect of He and H is paramount to understand the response of W to plasma exposures and neutron irradiations. OKMC has also been used to study the evolution of W in the presence of these two light elements. For this end, parameterizations of the behavior of these elements and their interactions among them and with V and SIA have been developed. Becquart et al. (2010) used their parametrization to study the isochronal annealing of He desorption in W and compared the results to experimental observations, employing the LAKIMOKA OKMC code (Domain et al. 2004). Subsequently, they studied the microstructural evolution of W under irradiation accounting for He production. They observe that the OKMC model reproduces satisfactorily the microstructure formed in the track region by 800 ^{3}He implantation for different fluence conditions (see Fig. 8).

The influence of grain boundaries on the microstructure evolution accounting for He has also been studied within an OKMC model. Extending the parametrization of Becquart et al. (Becquart and Domain 2009; Becquart et al. 2010), Valles et al. (2015a, b) studied the retention of He in the sample depending on the density of grain boundaries under pulsed He irradiation. They observe that around 50% of the incoming ions were retained at the interfaces in nanocrystalline W, while in the case of larger grains, that number dropped to around 30%, which indicates a strong dependence of He retention with grain boundary configurations. They also conclude that in the nanocrystalline W, mixed $\mathrm{He}_n\mathrm{V}_m$ clusters contain more vacancies with a lower He/V ratio.

Valles et al. (2017a) have also studied the influence of H atoms in the defect evolution under irradiation and the effect of grain boundaries in the sample. They

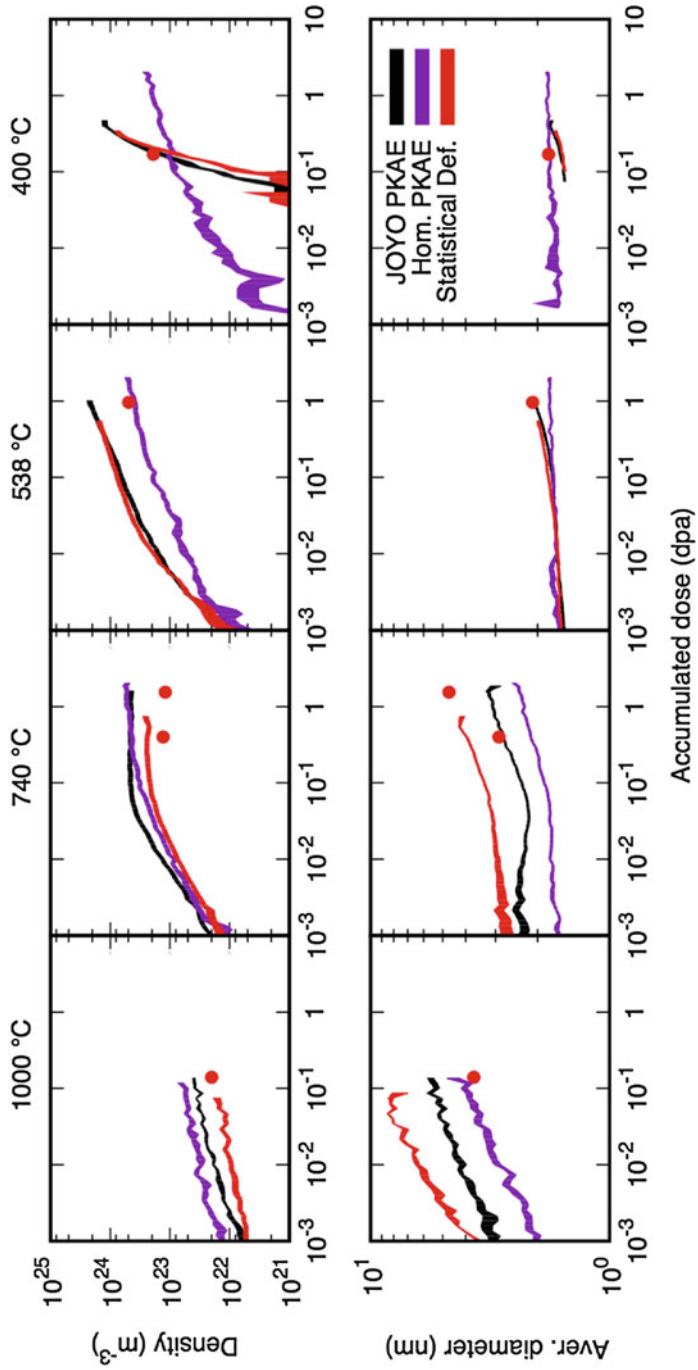

Fig. 7 Evolution with the accumulated dose of the void density and average void diameter found in OKMC simulations, as compared to experimental evidence (red dots) (Castin et al. 2017)

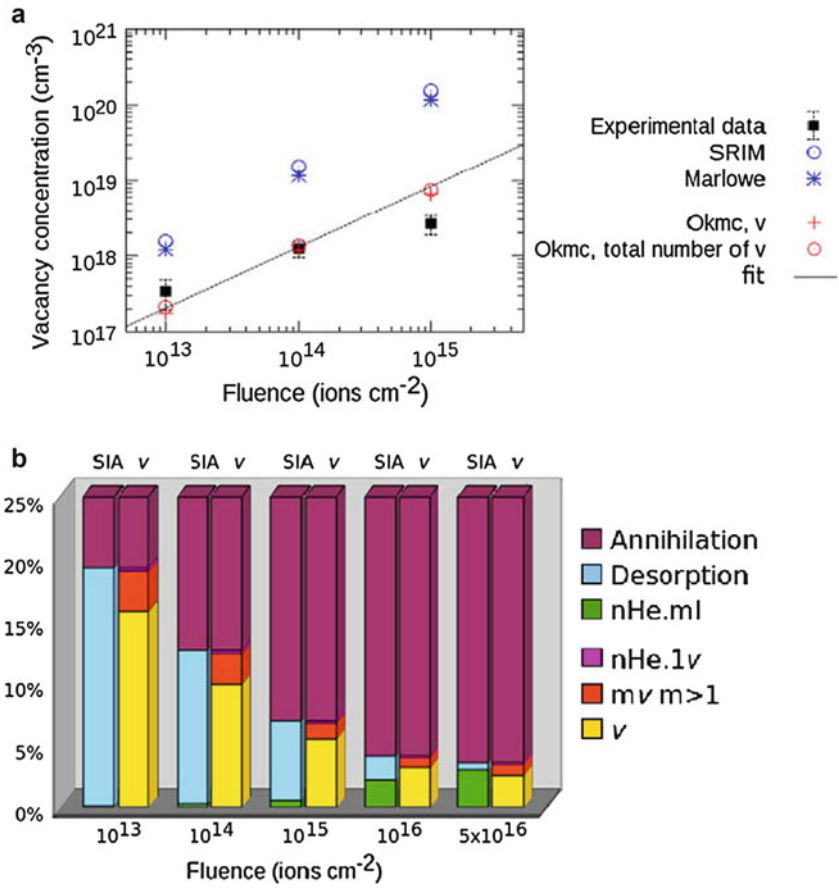

Fig. 8 (**a**) Vacancy concentration at the end of the implantation sequence for different fluences: a comparison of the experimental data with the SRIM, MARLOWE, or OKMC models. The black line is a linear fit (in the logarithmic scale) of the OKMC results. (**b**) The amount of desorption, annihilation, and clustering versus fluence at the end of the implantation stage as calculated by OKMC (Becquart et al. 2011)

extended the energetics for small clusters available in the literature (Henriksson et al. 2005; Fernandez et al. 2015; Lu et al. 2014; Ohsawa et al. 2010) to parametrize the H-V interactions using DFT calculations and considered H-SIA clusters as immobile. It is important to note that the H-H interaction is repulsive and, therefore, pure H clusters will not occur. However, in the presence of defects, the situation is different, with a strong binding between vacancies and H atoms. The authors conducted OKMC simulations using the MMonCa code (Martin-Bragado et al. 2013) and concluded that grain boundaries have a clear influence on the number density and distribution of vacancies, observing a larger concentration

in the nanocrystalline sample compared to a single-crystal sample. Also, they observed that H retention is highly influenced by both grain boundaries and vacancy concentration, the size of H_nV_m clusters varies slightly with the presence of grain boundaries, and grain boundaries act as fast diffusion pathways for H. Other KMC models on the same system reached similar conclusions (Oda et al. 2015).

Impurities, such as carbon and oxygen, or alloying elements or transmutation products will also influence the long-term damage evolution in W. DFT calculations have shown that both vacancies and He atoms strongly interact with solute atoms. Carbon and oxygen have also been found to be able to trap He atoms, increasing its retention in the material and the probability of forming bubbles. Self-interstitial atoms also interact with solute atoms and impurities (Suzudo et al. 2014; Gharaee et al. 2016; Huang et al. 2017, 2018). Some of these extra atoms modify the relative stability of SIA configurations, which in turn modifies the transport properties and the flux coupling between the defects and the solute elements. Very recently, Castin et al. (2018) have developed an OKMC model based on DFT calculations to study the role of carbon impurities in defect evolutions and also the presence of rhenium upon neutron irradiation, which also impacts the diffusivity of defects and therefore the microstructure evolution. Their model compares well with experiments in terms of both density of loops and voids.

Another material problem where the OKMC has been extensively applied was the analysis of the formation of a nanostructured surface morphology termed as fuzz appearing in W exposed to He plasma under conditions relevant for energy generation. The increased surface area and fragility of these nanostructured surfaces raise new concerns for the use of W as a fusion reactor PFM, particularly as a source of high-Z dust that will contaminate the plasma. Lasa et al. (2014) developed a model considering the He atoms and the bubbles as the objects in the system. He atoms are mobile but bubbles are not. Bubbles are considered to blast at a threshold distance from the surface that depends on the bubble radius. They concluded that the square root of time dependence of the growth rate is due to the He bubble growth and not to He diffusivity. The surface above the bubbles grows as interstitial loops are emitted from the bubbles with a preferential direction toward the surface. Bubble rupture near the surface will create roughness as seen in the experiments. Even though the model does not consider elastic interactions, nor surface diffusion or W knockout adatom formation, it reproduces the experimentally found growth dependence on time, which suggests that those mechanisms might not be crucial to explain fuzz formation. Building on this model, refining the parametrization, Valles et al. (2017b) studied the effect of temperature on fuzz growth. The authors identified the reason for fuzz formation as the formation of large He_nV_m clusters, which are only stable at intermediate temperatures (900–1900 K). At low temperatures (700 K), fuzz growth is prevented by the stability of small He_9V_1 clusters, hindering He emission. In contrast, at high temperatures (2500 K), fuzz does not grow due to the high He emission from He_nV_m clusters, leading to their dissolution and, thus, preventing He retention.

8 Limitations of the Method

The main limitation of the method is the fact that all possible mechanisms characterizing viable events have to be identified a priori and taken as input for the OKMC simulations. However, it is oftentimes the case that unforeseen mechanisms occur as the system evolves in time. One simple example often given in the literature is the adatom diffusion on a {100} free surface in fcc metals, which was long misunderstood until Feibelman showed that the exchange mechanism could be energetically favorable compared to direct migration (Feibelman 1990). Recent examples include the computational observation using MD that stacking fault tetrahedra (characteristic irradiation-created defects in fcc metals) might indeed migrate with diffusivities depending on their atomic structure, contrary to the commonly accepted assumption that described these defects as immobile (Martinez and Uberuaga 2015). It was shown that their mobility can significantly impact the long-term behavior of the system, precisely relying on an OKMC model as implemented in the code MMonCa (Martin-Bragado et al. 2013). Another interesting example is the understanding that small He clusters might indeed diffuse in a W matrix as Frenkel pairs are created and the self-interstitial annihilates with a different vacancy to the originally created, leading to net translation of the cluster. Using a cluster dynamics model as implemented in the code Xolotl (Xu et al. 2012), it was shown that the incorporation of this mechanism in the viable events significantly modifies the amount of He retained in the W wall and the bubble distribution. As the microstructure becomes more complex, the probability of finding new mechanisms increases, which might significantly modify the long-term evolution of the system (Uberuaga et al. 2018). Therefore, much attention needs to be given to understanding the atomistic processes occurring in the systems of interest under irradiation and their characterization with accurate rates for the OKMC calculations to be predictive.

It is also commonly assumed that the rates for the possible events are independent of the current configuration, i.e., there is no long-range interaction between defects that might modify their diffusivities. There are studies in the literature mitigating this limitation (Hudson et al. 2005; Wen et al. 2009; Subramanian et al. 2013; Mason et al. 2014). A common approach is to use a linear approximation in which the dipolar tensor of the defect is used to compute a variation of the energy at the saddle point and at the initial state due to elastic interactions (among defects and also between irradiation-created defects and pre-existing dislocations/grain boundaries (Vattré et al. 2016)). These modifications in the rates due to elastic interactions have been shown to modify the microstructural evolution of the system. A similar situation is encountered in the case of charged defects, in which long-range Coulomb interactions might be considered to bias defect diffusivities (Martin-Bragado et al. 2006). Although these long-range effects might be significant, they are not commonly considered based on computational arguments. Usually this problem scales as $O(N^2)$, with N the number of species, which reduces the efficiency of the algorithm and the attainable simulated time. This bottleneck could

be in part mitigated relying on fast multipole methods, which reduce the algorithmic complexity to $O(N)$ (Arsenlis et al. 2007), albeit with a large pre-factor, or Fourier transform methods ($n \log(n)$), with n the number of grid points (Hunter et al. 2011; Bertin et al. 2015), to accelerate the computation of the interactions.

In principle the method should be able to handle alloying elements and impurities provided that the whole parametrization is known. In practice this represents another challenge in terms of computation since the number of events can increase considerably. Also, the definition of local concentration and its relation with a certain cluster is unclear for non-dilute alloys. In this scenario, it is also important to consider the possibility of defect trapping, i.e., the presence of superbasins in which defects might flicker between nearby positions without much addition to the simulated time, reducing considerably the efficiency of the algorithm. Several methods have been proposed to alleviate this drawback that can indeed significantly increase the efficiency in such situations (Novotny 1995; Fichthorn and Lin 2013; Athènes and Bulatov 2014).

In common conditions in nuclear environments, the amount of irradiation-created defects per unit time and volume is considerable and increases with time until it reaches steady state (if attainable). Tracking all these defects in an efficient manner is a challenge. Parallel algorithms to take advantage of parallel architectures have been recently developed with the goal of improving both simulated time and system size (Shim and Amar 2005a, b; Martínez et al. 2008, 2011). Implementation on GPU architectures has also been considered with the same goal and showed promising results (Jiménez and Ortiz 2016).

9 Conclusions

We have reviewed in this chapter the kinetic Monte Carlo (KMC) methodology describing in detail the theory behind this powerful and flexible approach and how it can be used to study the microstructure evolution of systems under irradiation. The KMC approach described here is called object KMC (OKMC), which coarse-grains out the atomic structure to focus on elements (or objects) of interest, such as irradiation-created defects, impurities, transmutation or alloying elements, etc. These objects evolve in time according to prescribed rules characterized by probabilities per unit time (or rates), which enter in the OKMC algorithm to follow the system evolution. It is commonly assumed that the rates follow transition state theory, which relates activation free energies and attempt frequencies with such rates. We have seen how these parameters can be accurately calculated using density functional theory, which explicitly accounts for the electronic degrees of freedom. Although computationally expensive, which limits system size and total simulated time if dynamics are required, its accuracy, superior to that of empirical interatomic potentials makes it the method of choice to obtain the required values for single defects and small defect clusters, along with their interactions with impurities and alloying elements. We have shown two examples in which the evolution of the

system under irradiation has been studied using this methodology: ferritic steels and tungsten. In both systems we show that the results in terms of defect distributions can be satisfactorily compared to experimental observations. Finally, we have reviewed the limitations of the methodology and how current research approaches are tackling those limitations.

Acknowledgments The authors thank Malvin H. Kalos, Alfredo Caro, Frédéric Soisson, Vasily Bulatov, Blas Uberuaga, Arthur F. Voter, and Danny Perez for many useful discussions. E.M. wants to thank Gustavo Esteban for useful comments on the manuscript. E.M. acknowledges the support of the U.S. DOE, Office of Science, Advanced Scientific Computing Research and Fusion Energy Sciences through the Scientific Discovery through Advanced Computing (SciDAC) project on Plasma-Surface Interactions for this work. This research used resources provided by the LANL Institutional Computing Program. LANL, an affirmative action/equal opportunity employer, is operated by Los Alamos National Security, LLC, for the National Nuclear Security Administration of the US DOE under contract DE-AC52-06NA25396.

References

Abe H, Kuramoto E (1999) Interaction of solutes with irradiation-induced defects of electron-irradiated dilute iron alloys. J Nucl Mater 271–272:209–213

Arsenlis A, Cai W, Tang M, Rhee M, Oppelstrup T, Hommes G, Pierce TG, Bulatov VV (2007) Enabling strain hardening simulations with dislocation dynamics. Model Simul Mater Sci Eng 15:553–595

Athènes M, Bulatov VV (2014) Path factorization approach to stochastic simulations. Phys Rev Lett 113(23):230601

Baldwin M, Doerner R (2008) Helium induced nanoscopic morphology on tungsten under fusion relevant plasma conditions. Nucl Fusion 48(3):035001, 00193

Becke AD (1988) Density-functional exchange-energy approximation with correct asymptotic-behavior. Phys Rev A 38(6):3098–3100

Becquart CS, Domain C (2007) Ab initio calculations about intrinsic point defects and He in W. Nucl Instrum Methods Phys Res Sect B Beam Interact Mater Atoms 255(1):23–26

Becquart CS, Domain C (2009) A density functional theory assessment of the clustering behaviour of He and H in tungsten. J Nucl Mater 386–388:109–111

Becquart CS, Domain C (2010) Modeling microstructure and irradiation effects. Metall Mater Trans A 42A:852

Becquart CS, Domain C, Sarkar U, DeBacker A, Hou M (2010) Microstructural evolution of irradiated tungsten: ab initio parameterisation of an OKMC model. J Nucl Mater 403(1–3): 75–88

Becquart CS, Barthe MF, De Backer A (2011) Modelling radiation damage and He production in tungsten. Phys Scripta T145:014048

Bertin N, Upadhyay MV, Pradalier C, Capolungo L (2015) A FFT-based formulation for efficient mechanical fields computation in isotropic and anisotropic periodic discrete dislocation dynamics. Model Simul Mater Sci Eng 23(6):065009

Bortz AB, Kalos MH, Lebowitz JL (1975) A new algorithm for Monte Carlo simulation of Ising spin systems. J Comput Phys 17:10–18

Castin N, Bakaev A, Bonny G, Sand A, Malerba L, Terentyev D (2017) On the onset of void swelling in pure tungsten under neutron irradiation: an object kinetic Monte Carlo approach. J Nucl Mater 493:280–293

Castin N, Bonny G, Bakaev A, Ortiz C, Sand A, Terentyev D (2018) Object kinetic Monte Carlo model for neutron and ion irradiation in tungsten: impact of transmutation and carbon impurities. J Nucl Mater 500:15–25

Caturla MJ, Soneda N, Alonso E, Wirth BD, Diaz de la Rubia T, Perlado JM (2000) Comparative study of radiation damage accumulation in Cu and Fe. J Nucl Mater 276:13

Ceperley DM, Alder BJ (1980) Ground state of the electron gas by a stochastic method. Phys Rev Lett 45(7):4

Chatterjee A, Vlachos DG (2007) An overview of spatial microscopic and accelerated kinetic Monte Carlo methods. J Comput-Aided Mater Des 14(2):253–308

Correa AA, Kohanoff J, Artacho E, Sánchez-Portal D, Caro A (2012) Nonadiabatic forces in ion-solid interactions: the initial stages of radiation damage. Phys Rev Lett 108(21):213201

Dai Y, Victoria M (1997) Defect cluster structure and tensile properties of copper single crystals irradiated with 600 MeV protons. MRS Proc 439:319–324

De Backer A, Sand A, Ortiz CJ, Domain C, Olsson P, Berthod E, Becquart CS (2016) Primary damage in tungsten using the binary collision approximation, molecular dynamic simulations and the density functional theory. Phys Scripta T167:014018

Domain C, Becquart CS, Malerba L (2004) Simulation of radiation damage in Fe alloys: an object kinetic Monte Carlo approach. J Nucl Mater 335:121

Draeger EW, Andrade X, Gunnels JA, Bhatele A, Schleife A, Correa AA (2017) Massively parallel first-principles simulation of electron dynamics in materials. J Parallel Distrib Comput 106: 205–214

Elcock EW (1959) Vacancy diffusion in ordered alloys. Proc Phys Soc 73:250

Elcock EW, McCombie CW (1958) Vacancy diffusion in binary ordered alloys. Phys Rev 109:605

El-Mellouhi F, Mousseau N, Lewis LJ (2008) Kinetic activation-relaxation technique: an off-lattice self-learning kinetic Monte Carlo algorithm. Phys Rev B 78:153202

Eyring H, Walter J, Kimball GE (1944) Quantum chemistry, 1st edn. Wiley, New York

Feibelman PJ (1990) Diffusion path for an Al adatom on Al(001). Phys Rev Lett 65(6):729–732

Fernandez N, Ferro Y, Kato D (2015) Hydrogen diffusion and vacancies formation in tungsten: density functional theory calculations and statistical models. Acta Mater 94:307–318

Fichthorn KA, Lin Y (2013) A local superbasin kinetic Monte Carlo method. J Chem Phys 138(16):164104

Fu CC, Dalla Torre J, Willaime F, Bocquet J-L, Barbu A (2005) Multiscale modelling of defect kinetics in irradiated iron. Nature Mater 4:68

Gámez L, Gámez B, Caturla MJ, Terentyev D, Perlado JM (2011) Object Kinetic Monte Carlo calculations of irradiated Fe-Cr dilute alloys: the effect of the interaction radius between substitutional Cr and self-interstitial Fe. Nucl Instrum Methods Phys Res Sect B Beam Interact Mater Atoms 269(14):1684–1688

Gharaee L, Marian J, Erhart P (2016) The role of interstitial binding in radiation induced segregation in W-Re alloys. J Appl Phys 120(2):025901

Gibson MA, Bruck J (2000) Efficient exact stochastic simulation of chemical systems with many species and many channels. J Phys Chem A 104(9):1876–1889

Gillespie D (1976) A general method for numerically simulating the stochastic time evolution of coupled chemical reactions. J Comput Phys 22:403–434

Gillespie D (1977) Exact stochastic simulation of coupled chemical reactions. J Phys Chem 81:2340–2361

Gilmer GH, Bennema P (1972) Simulation of crystal growth with surface diffusion. J Appl Phys 43(4):1347–1360

Glensk A, Grabowski B, Hickel T, Neugebauer J (2015) Understanding anharmonicity in fcc materials: from its origin to ab initio strategies beyond the quasiharmonic approximation. Phys Rev Lett 114(19):195901

Grabowski B, Hickel T, Neugebauer J (2007) Ab initio study of the thermodynamic properties of nonmagnetic elementary fcc metals: exchange-correlation-related error bars and chemical trends. Phys Rev B 76(2):024309

Grabowski B, Hickel T, Neugebauer J (2011) Formation energies of point defects at finite temperatures. Phys Status Solidi B 248(6):1295–1308. https://doi.org/10.1002/pssb.201046302

Hanusse P, Blanche A (1981) A Monte Carlo method for large reaction diffusion systems. J Chem Phys 74:6148

Heinisch HL (1990) Computer simulation of high energy displacement cascades. Radiat Eff Defects Solids 113:53
Henkelman G, Jonsson H (1999) A dimer method for finding saddle points on high dimensional potential surfaces using only first derivatives. J Chem Phys 111(15):7010–7022
Henkelman G, Jonsson H (2000) Improved tangent estimate in the nudged elastic band method for finding minimum energy paths and saddle points. J Chem Phys 113(22) 9978–9985
Henkelman G, Jonsson H (2001) Long time scale kinetic Monte Carlo simulations without lattice approximation and predefined event table. J Chem Phys 115(21):9657
Henkelman G, Uberuaga BP, Jonsson H (2000) A climbing image nudged elastic band method for finding saddle points and minimum energy paths. J Chem Phys 113(22):9901–9904
Henriksson KOE, Nordlund K, Krasheninnikov A, Keinonen J (2005) Difference in formation of hydrogen and helium clusters in tungsten. Appl Phys Lett 87(16):163113
Hohenberg P, Kohn W (1964) Inhomogenous electron gas. Phys Rev B 136:864–871
Huang G-Y, Juslin N, Wirth BD (2016) First-principles study of vacancy, interstitial, noble gas atom interstitial and vacancy clusters in bcc-W. Comput Mater Sci 123:121–130
Huang CH, Gharaee L, Zhao Y, Erhart P, Marian J (2017) Mechanism of nucleation and incipient growth of Re clusters in irradiated W-Re alloys from kinetic Monte Carlo simulations. Phys Rev B 96:094108
Huang CH, Gilbert MR, Marian J (2018) Simulating irradiation hardening in tungsten under fast neutron irradiation including Re production by transmutation. J Nucl Mat 499:204–215
Hudson TS, Dudarev SL, Caturla MJ, Sutton AP (2005) Effects of elastic interactions on post-cascade radiation damage evolution in kinetic monte carlo simulations. Philos Mag 85:661–675
Hunter A, Saied F, Le C, Koslowski M (2011) Large-scale 3D phase field dislocation dynamics simulations on high-performance architectures. Int J High Perform Comput Appl 25(2): 223–235
Jiménez F, Ortiz C (2016) A GPU-based parallel object kinetic monte carlo algorithm for the evolution of defects in irradiated materials. Comput Mater Sci 113:178–186
Kampen NGV (1992) Stochastic processes in physics and chemistry, 2nd edn. Elsevier, Amsterdam
Kohn W, Sham LJ (1965) Self-consistent equations including exchange and correlation effects. Phys Rev 140(4A):1133
Körmann F, Dick A, Grabowski B, Hallstedt B, Hickel T, Neugebauer J (2008) Free energy of bcc iron: integrated ab initio derivation of vibrational, electronic, and magnetic contributions. Phys Rev B 78(3):033102
Langreth DC, Mehl MJ (1983) Beyond the local-density approximation in calculations of ground-state electronic properties. Phys Rev B 28(4):1809–1834
Lasa A, Tahtinen SK, Nordlund K (2014) Loop punching and bubble rupture causing surface roughening A model for W fuzz growth. EPL (Europhys Lett) 105(2):25002, 00010
Lu G-H, Zhou H-B, Becquart CS (2014) A review of modelling and simulation of hydrogen behaviour in tungsten at different scales. Nucl Fusion 54(8):086001
Malerba L, Caro A, Wallenius J (2008) Multiscale modelling of radiation damage and phase transformations: The challenge of FeCr alloys. J Nucl Mater 382:112–125
Martin-Bragado I, Tian S, Johnson M, Castrillo P, Pinacho R, Rubio J, Jaraiz M (2006) Modeling charged defects, dopant diffusion and activation mechanisms for TCAD simulations using kinetic Monte Carlo. Nucl Instrum Methods Phys Res Sect B Beam Interact Mater Atoms 253(1–2):63–67
Martin-Bragado I, Rivera A, Valles G, Gomez-Selles JL, Caturla MJ (2013) MMonCa: an object kinetic Monte Carlo simulator for damage irradiation evolution and defect diffusion. Comput Phys Commun 184(12):2703–2710
Martinez E, Uberuaga BP (2015) Mobility and coalescence of stacking fault tetrahedra in Cu. Sci Rep 5:9084
Martínez E, Marian J, Kalos M, Perlado J (2008) Synchronous parallel kinetic Monte Carlo for continuum diffusion-reaction systems. J Comput Phys 227(8):3804–3823
Martínez E, Monasterio PR, Marian J (2011) Billion-atom synchronous parallel kinetic Monte Carlo simulations of critical 3D Ising systems. J Comp Phys 230:1359–1369

Mason DR, Yi X, Kirk MA, Dudarev SL (2014) Elastic trapping of dislocation loops in cascades in ion-irradiated tungsten foils. J Phys Condens Matter 26(37):375701

Maury F, Lucasson P, Lucasson A, Faudot F, Bigot J (1987) A study of irradiated FeCr alloys: deviations from Matthiessen's rule and interstitial migration. J Phys F Metal Phys 17(5): 1143–1165

Nguyen-Manh D, Dudarev S (2006) Multi-scale modelling of defect behavior in BCC transition metals and iron alloys for future fusion power plants. Mater Sci Eng A 423(1–2): 74–78

Niklasson A, Tymczak C, Challacombe M (2006) Time-reversible born-oppenheimer molecular dynamics. Phys Rev Lett 97(12):123001

Novotny MA (1995) Monte Carlo algorithms with absorbing Markov chains: fast local algorithms for slow dynamics. Phys Rev Lett 74(1):1

Oda T, Zhu D, Watanabe Y (2015) Kinetic Monte Carlo simulation on influence of vacancy on hydrogen diffusivity in tungsten. J Nucl Mater 467:439–447

Ohsawa K, Goto J, Yamakami M, Yamaguchi M, Yagi M (2010) Trapping of multiple hydrogen atoms in a tungsten monovacancy from first principles. Phys Rev B 82(18):184117

Olsson P (2009) Ab initio study of interstitial migration in Fe-Cr alloys. J Nucl Mater 386–388: 86–89

Olsson P, Domain C, Wallenius J (2007) Ab initio study of Cr interactions with point defects in bcc Fe. Phys Rev B 75:014110

Olsson P, Becquart CS, Domain C (2016) Ab initio threshold displacement energies in iron. Mater Res Lett 4(4):219–225

Opplestrup T, Bulatov V, Gilmer G, Kalos M, Sadigh B (2006) First-passage Monte Carlo algorithm: diffusion without all the Hops. Phys Rev Lett 97(23):230602

Perdew JP, Chevary JA, Vosko SH, Jackson KA, Pederson MR, Singh DJ, Fiolhais C (1992) Atoms, molecules, solids, and surfaces: applications of the generalized gradient approximation for exchange and correlation. Phys Rev B 46(11):6671–6687

Perini A, Jacucci G, Martin G (1984) Cluster free energy in the simple-cubic Ising model. Phys Rev B 29(5):2689–2697

Schulze TP (2002) Kinetic Monte Carlo simulations with minimal searching. Phys Rev E 65(3):036704

Shim Y, Amar J (2005a) Rigorous synchronous relaxation algorithm for parallel kinetic Monte Carlo simulations of thin film growth. Phys Rev B 71(11):115436

Shim Y, Amar JG (2005b) Semirigorous synchronous sublattice algorithm for parallel kinetic Monte Carlo simulations of thin film growth. Phys Rev B 71:125432

Sholl DS, Steckel JA (2009) Density functional theory - A practical introduction. Wiley, Hoboken

Slepoy A, Thompson AP, Plimpton SJ (2008) A constant-time kinetic Monte Carlo algorithm for simulation of large biochemical reaction networks. J Chem Phys 128(20):205101

Söderlind P, Yang LH, Moriarty JA, Wills JM (2000) First-principles formation energies of monovacancies in bcc transition metals. Phys Rev B 61(4):2579–2586

Sørensen MR, Voter AF (2000) Temperature-accelerated dynamics for simulation of infrequent events. J Chem Phys 112(21):9599–9606

Subramanian G, Perez D, Uberuaga BP, Tomé CN, Voter AF (2013) Method to account for arbitrary strains in kinetic Monte Carlo simulations. Phys Rev B 87(14):144107

Suzudo T, Yamaguchi M, Hasegawa A (2014) Stability and mobility of rhenium and osmium in tungsten: first principles study. Model Simul Mater Sci Eng 22(7):075006

Takaki S, Fuss J (1983) Dedek HKU, Schultz H. The resistivity recovery of high purity and carbon doped iron following low electron irradiation. Rad Eff 79:87–122

Trushin O, Karim A, Kara A, Rahman TS (2005) Self-learning kinetic Monte Carlo method: application to Cu(111). Phys Rev B 72:115401

Uberuaga BP, Hoagland RG, Voter AF, Valone SM (2007) Direct Transformation of Vacancy Voids to Stacking Fault Tetrahedra. Phys Rev Lett 99:135501

Uberuaga BP, Martínez E, Perez D, Voter AF (2018) Discovering mechanisms relevant for radiation damage evolution. Comput Mater Sci 147:282–292

Valles G, González C, Martin-Bragado I, Iglesias R, Perlado J, Rivera A (2015a) The influence of high grain boundary density on helium retention in tungsten. J Nucl Mater 457:80–87

Valles G, Cazalilla AL, Gonzalez C, Martin-Bragado I, Prada A, Iglesias R, Perlado J, Rivera A (2015b) A multiscale approach to defect evolution in tungsten under helium irradiation. Nucl Instrum Methods Phys Res Sect B Beam Interact Mater Atoms 352:100–103

Valles G, Panizo-Laiz M, González C, Martin-Bragado I, González-Arrabal R, Gordillo N, Iglesias R, Guerrero C, Perlado J, Rivera A (2017a) Influence of grain boundaries on the radiation-induced defects and hydrogen in nanostructured and coarse-grained tungsten. Acta Mater 122:277–286

Valles G, Martin-Bragado I, Nordlund K, Lasa A, Björkas C, Safi E, Perlado J, Rivera A (2017b) Temperature dependence of underdense nanostructure formation in tungsten under helium irradiation. J Nucl Mater 490:108–114

Vattré A, Jourdan T, Ding H, Marinica M-C, Demkowicz MJ (2016) Non-random walk diffusion enhances the sink strength of semicoherent interfaces. Nat Commun 7:10424

Vineyard GH (1957) Frequency factors and isotope effects in solid state rate processes. J Phys Chem Solids 3(1–2):121–127

Voter AF (1997) Hyperdynamics: accelerated molecular dynamics of infrequent events. Phys Rev Lett 78(20):3908

Voter AF (1998) Parallel replica method for dynamics of infrequent events. Phys Rev B 57(22):R13985

Voter AF (2007) Introduction to the kinetic Monte Carlo method, Ch. 1. Springer, Dordrecht

Voter AF, Doll JD (1984) Transition state theory description of surface self-diffusion: comparison with classical trajectory results. J Chem Phys 80:5832

Voter AF, Doll JD (1985) Dynamical corrections to transition state theory for multistate systems: surface self-diffusion in the rare-event regime. J Chem Phys 82:80–92

Was GS (2007) Fundamentals of radiation materials science. Springer, Berlin/Heidelberg/New York

Wen M, Takahashi A, Ghoniem NM (2009) Kinetics of self-interstitial cluster aggregation near dislocations and their influence on hardening. J Nucl Mater 392:386–395

Witt WC, del Rio BG, Dieterich JM, Carter EA (2018) Orbital-free density functional theory for materials research. J Mater Res 33:1–19

Xu L, Henkelman G (2008) Adaptive kinetic Monte Carlo for first-principles accelerated dynamics. J Chem Phys 129:114104

Xu D, Wirth BD, Li M, Kirk MA (2012) Defect microstructural evolution in ion irradiated metallic nanofoils: kinetic Monte Carlo simulation versus cluster dynamics modeling and in situ transmission electron microscopy experiments. Appl Phys Lett 101(10):101905

Young WM, Elcock EW (1966) Monte Carlo studies of vacancy migration in binary ordered alloys: I. Proc Phys Soc 89:735

Zhang J, Zhang H, Ye H, Zheng Y (2016) Free-end adaptive nudged elastic band method for locating transition states in minimum energy path calculation. J Chem Phys 145(9):094104

Zhu T, Li J, Samanta A, Kim HG, Suresh S (2007) Interfacial plasticity governs strain rate sensitivity and ductility in nanostructured metals. Proc Natl Acad Sci 104(9):3031–3036

Zinkle SJ, Farrell K (1989) Void swelling and defect cluster formation in reactor-irradiated copper. J Nucl Mater 168:262–267